Supporting Information

The influence of diameter of multiwalled carbon nanotubes on mechanical, optical and electrical properties of Langmuir-Schaefer films

Karol Rytel*[a], Kamil Kędzierski[a], Bolesław Barszcz[b], Małgorzata Widelicka[b], Alicja Stachowiak[a], Andrzej Biadasz[a], Łukasz Majchrzycki[c], Emerson Coy[d], Danuta Wróbel[a]

[a]Faculty of Materials Engineering and Technical Physics, Institute of Physics, Poznan University of Technology, Piotrowo 3, 60-965 Poznań, Poland
[b]Institute of Molecular Physics, Polish Academy of Sciences, Smoluchowskiego 17, 60-179 Poznań, Poland
[c]Centre for Advanced Technology, Adam Mickiewicz University, Uniwersytetu Poznańskiego 10, 60-780 Poznań, Poland
[d]NanoBioMedical Centre, Adam Mickiewicz University, Umultowska 85, 61-614 Poznań, Poland

Oscillatory Barrier Measurements

During one measurement following three signals with full 10 cycles was registered: surface pressure measured in parallel direction vs. time (**$\Pi_{||}$ vs. t**), surface pressure measured in perpendicular direction vs time (**$\Pi_{\perp}$ vs t**) and area between the barriers vs. time (**A vs. t**). To determine the **ΔA** and **ΔΠ** amplitudes and phase shifts **φ** Origin 8.1 sine fit function was used for all obtained signals:

$$y = y_0 + Csin\left(\pi\frac{x - x_c}{w}\right), (S1)$$

To provide better clarity the subscript contains information (|| for **$\Pi_{||}$ vs t**; ⊥ for **$\Pi_{\perp}$ vs t; A** for **A vs t)** about the signal from which the data were obtained. The value of **φ** and the phase shifts error **Δ φ** were defined as follows:

$$\varphi_{||} = \left(\frac{x_{c||}}{w_{||}} - \frac{x_{cA}}{w_A}\right)\pi - \pi, (S2)$$

$$\Delta\varphi_{||} = \left|\frac{\Delta x_{c||}}{w_{||}}\pi\right| + \left|\frac{\Delta x_{cA}}{w_A}\pi\right| + \left|\frac{x_{c||}}{w_{||}^2}\Delta w_{||}\pi\right| + \left|\frac{x_{cA}}{w_A^2}\Delta w_A\pi\right|, (S3)$$

$$\varphi_{\perp} = \left(\frac{x_{c\perp}}{w_{\perp}} - \frac{x_{cA}}{w_A}\right)\pi - \pi, (S3)$$

$$\Delta\varphi_{\perp} = \left|\frac{\Delta x_{c\perp}}{w_{\perp}}\pi\right| + \left|\frac{\Delta x_{cA}}{w_A}\pi\right| + \left|\frac{x_{c\perp}}{w_{\perp}^2}\Delta w_{\perp}\pi\right| + \left|\frac{x_{cA}}{w_A^2}\Delta w_A\pi\right|. (S3)$$

Because reducing the area between the barriers leads to an increase in surface pressure and the signal A vs. t is shifted in phase by π in relation to the barrier position vs. time in equation S2 and S3 we subtract π.

The real part of compression modulus and its measurement error can be defined as:

$$\varepsilon' = \frac{|\varepsilon^* + G^*|cos(\varphi_{||}) + |\varepsilon^* - G^*|cos(\varphi_{\perp})}{2}, (S4)$$

$$\Delta\varepsilon' = \left|\frac{1}{2}cos(\varphi_{||})\,\Delta|\varepsilon^* + G^*|\right| + \left|\frac{1}{2}cos(\varphi_{\perp})\,\Delta|\varepsilon^* - G^*|\right| + \left|\frac{1}{2}|\varepsilon^* + G^*|\,sin(\varphi_{||})\,\Delta\varphi_{||}\right| + \left|\frac{1}{2}|\varepsilon^* - G^*|\,sin(\varphi_{\perp})\,\Delta\varphi_{\perp}\right|, (S5)$$

The real part of shear modulus and its measurement error can be defined as:

$$G' = \frac{|\varepsilon^* + G^*|\,cos(\varphi_{||}) - |\varepsilon^* - G^*|\,cos(\varphi_{\perp})}{2}, (S6)$$

$$\Delta G' = \left|\frac{1}{2}cos(\varphi_{||})\,\Delta|\varepsilon^* + G^*|\right| + \left|\frac{1}{2}cos(\varphi_{\perp})\,\Delta|\varepsilon^* - G^*|\right| + \left|\frac{1}{2}|\varepsilon^* + G^*|\,sin(\varphi_{||})\,\Delta\varphi_{||}\right| + \left|\frac{1}{2}|\varepsilon^* - G^*|\,sin(\varphi_{\perp})\,\Delta\varphi_{\perp}\right|, (S7)$$

The imaginary part of compression modulus and its measurement error can be defined as:

$$\varepsilon'' = \frac{|\varepsilon^* + G^*|sin(\varphi_{||}) + |\varepsilon^* - G^*|sin(\varphi_{\perp})}{2}, (S8)$$

$$\Delta\varepsilon'' = \left|\frac{1}{2}sin(\varphi_{||})\,\Delta|\varepsilon^* + G^*|\right| + \left|\frac{1}{2}sin(\varphi_{\perp})\,\Delta|\varepsilon^* - G^*|\right| + \left|\frac{1}{2}|\varepsilon^* + G^*|\,cos(\varphi_{||})\,\Delta\varphi_{||}\right| + \left|\frac{1}{2}|\varepsilon^* - G^*|\,cos(\varphi_{\perp})\,\Delta\varphi_{\perp}\right|. (S9)$$

The imaginary part of shear modulus and its measurement error can be defined as:

$$G'' = \frac{|\varepsilon^* + G^*|\,sin(\varphi_{||}) - |\varepsilon^* - G^*|\,sin(\varphi_{\perp})}{2}, (S10)$$

$$\Delta G'' = \left|\frac{1}{2}sin(\varphi_{||})\,\Delta|\varepsilon^* + G^*|\right| + \left|\frac{1}{2}sin(\varphi_{\perp})\,\Delta|\varepsilon^* - G^*|\right| + \left|\frac{1}{2}|\varepsilon^* + G^*|\,cos(\varphi_{||})\,\Delta\varphi_{||}\right| + \left|\frac{1}{2}|\varepsilon^* - G^*|\,cos(\varphi_{\perp})\,\Delta\varphi_{\perp}\right|, (S11)$$

Where:

$$|\varepsilon^* + G^*| = A_0\frac{\Delta\Pi_{||}}{\Delta A} = \frac{y_{0A}C_{||}}{C_A}, (S12)$$

$$\Delta|\varepsilon^* + G^*| = \left(\frac{\Delta y_{0A}}{y_{0A}} + \frac{\Delta C_{||}}{C_{||}} + \frac{\Delta C_A}{C_A}\right) * |\varepsilon^* + G^*|, (S13)$$

$$|\varepsilon^* - G^*| = A_0\frac{\Delta\Pi_{\perp}}{\Delta A} = \frac{y_{0A}C_{\perp}}{C_A}, (S14)$$

$$\Delta|\varepsilon^* - G^*| = \left(\frac{\Delta y_{0A}}{y_{0A}} + \frac{\Delta C_{\perp}}{C_{\perp}} + \frac{\Delta C_A}{C_A}\right) * |\varepsilon^* - G^*|, (S15)$$

The measurement error of obtained compression and shear modulii (presented in Table 2 in main text) appear to be very low. It was decided to check how much reproducible results will be obtained for the layers obtained from MWCNT 9 sample. The results of four independent measurements were shown in Table S1. Most of the received results were within the limits of the measurement uncertainty and the deviations that occur were originated from the inhomogeneity of the layer formed after MWCNT suspension has been applied on the air water interface. The measurement of layer designated as MWCNT 9 was selected for analysis

in the main text due to the lowest uncertainty of measurement and the closest to sinusoidal signals $\Pi_{||}$ **vs. t** and $\Pi_{\perp}$ **vs t**.

Table S1 The mechanical parameters of the Langmuir films obtained from the powder labeled as MWCNT 9

Film name	**ε'** [mN m^{-1}]	**ε''** [mN m^{-1}]	**G'** [mN m^{-1}]	**G''** [mN m^{-1}]
MWCNT 9	171.9 ± 1.3	59.5 ± 1.1	71.3 ± 1.1	23.6 ± 1.1
MWCNT 9.2	175.9 ± 3.2	61.0 ± 3.2	66.4 ± 3.3	19.7 ± 3.2
MWCNT 9.3	175 ± 3	62 ± 2	65 ± 5	19.9 ± 1.7
MWCNT 9.4	173.3 ± 1.5	62.9 ± 1.3	67.1 ± 1.5	21.6 ± 1.4

UV-Vis spectra

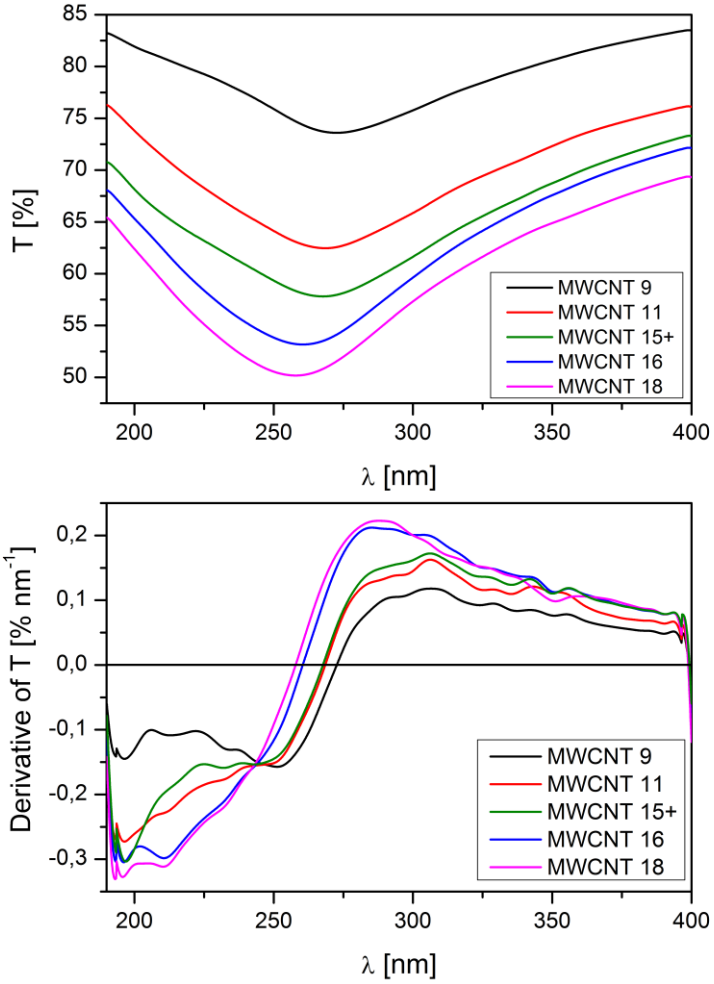

Fig. S1 UV transmittance spectra recorded at 0.3 nm step (top) and its derivative (bottom)

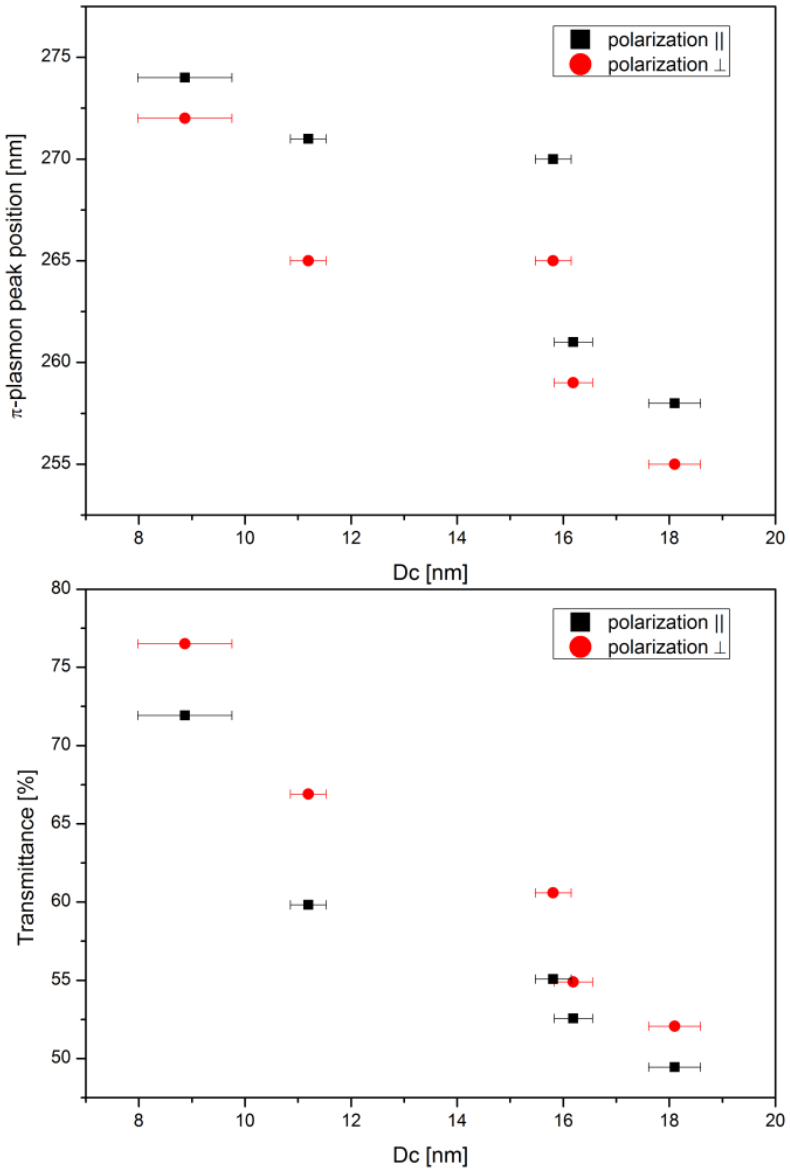

Fig. S2 Plasmon band position (top) and corresponding transmittance value (bottom) vs. diameter of the used MWCNT for electric vector polarization parallel and perpendicular to the barrier orientation

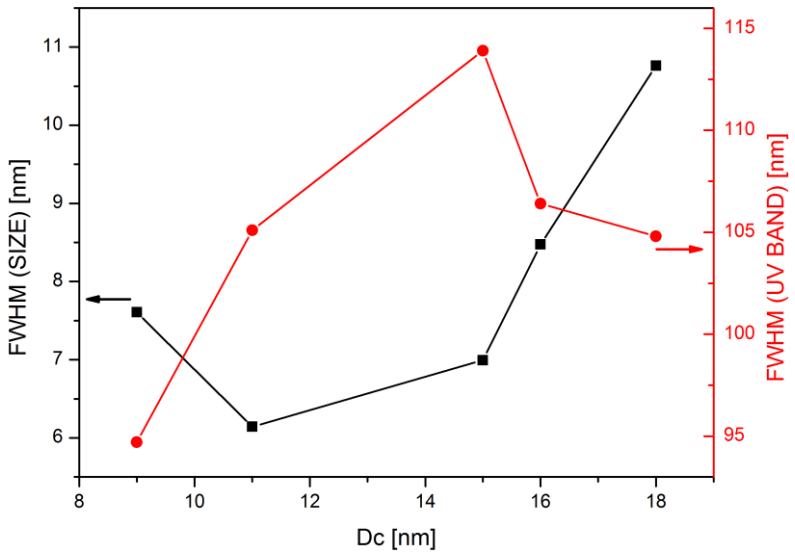

Fig. S3 The full width at half maximum (FWHM) of UV bands and diameter size

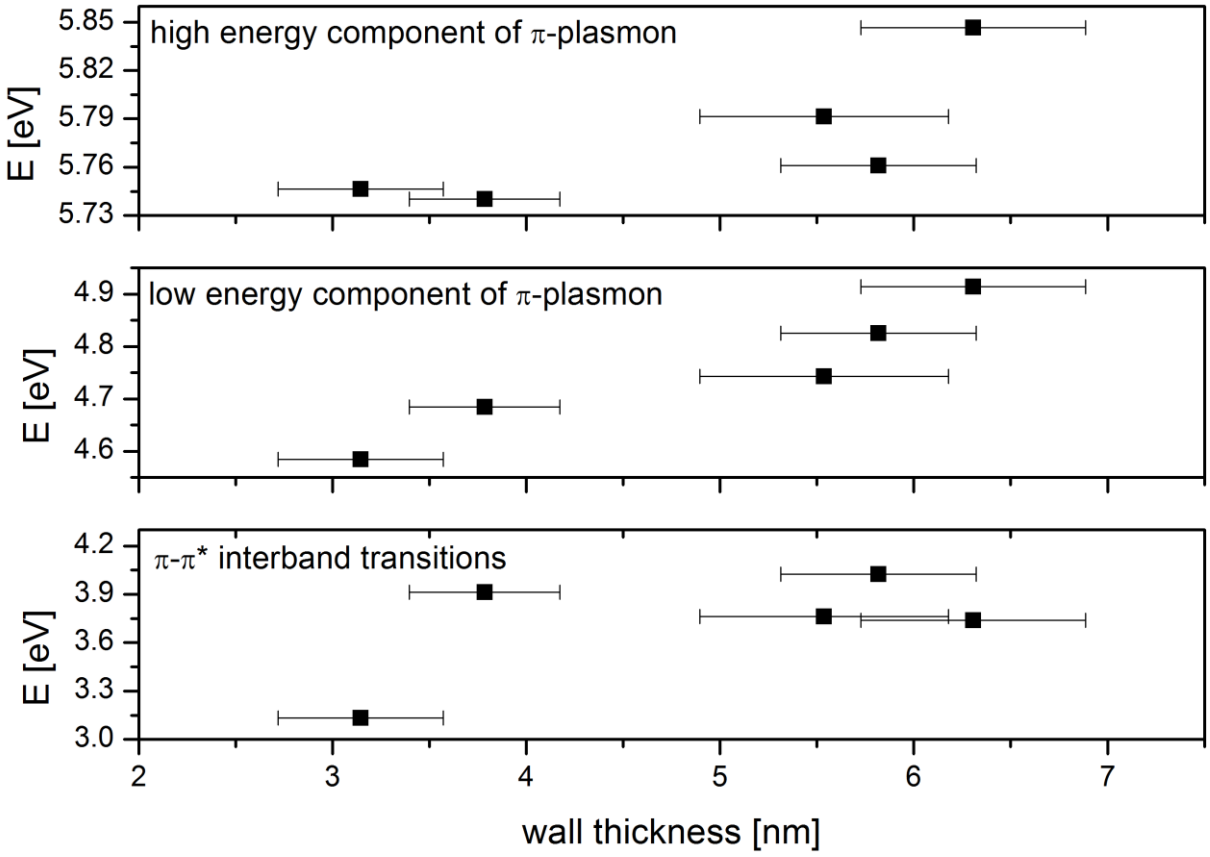

Fig. S4 Position of MWCNT UV-Vis spectra components vs wall thickness

Raman spectra

Table S2 Band position in Raman spectra

Sample name	Powder				Layer			
	D [cm^{-1}]	G [cm^{-1}]	D' [cm^{-1}]	2D [cm^{-1}]	D [cm^{-1}]	G [cm^{-1}]	D' [cm^{-1}]	2D [cm^{-1}]
MCWNT 9	1326.60	1577.05	1609.27	2646.09	1332.46	1584.02	1617.26	2658.14
MCWNT 11	1328.74	1578.55	1610.87	2649.22	1332.74	1584.53	1617.10	2658.26
MCWNT15+	1326.74	1575.58	1608.98	2649.92	1333.02	1583.76	1618.06	2659.69
MCWNT 16	1327.81	1579.16	1610.57	2649.59	1333.27	1586.56	1618.23	2660.13
MCWNT 18	1328.69	1580.24	1610.55	2649.73	1333.15	1585.84	1617.4	2659.31

Table S3 Band parameters of Raman spectra

Sample name	Powder				Layer			
	I_D/I_G	A_D/A_G	$I_D/I_{D'}$	$A_D/A_{D'}$	I_D/I_G	A_D/A_G	$I_D/I_{D'}$	$A_D/A_{D'}$
MCWNT 9	1.89150	2.46849	2.75314	7.03301	1.85234	2.26223	2.64812	7.00032
MCWNT 11	1.90435	2.23033	2.99555	6.06936	2.17196	2.47627	3.06349	7.9948
MCWNT15+	1.86665	2.32679	3.42811	6.47527	1.78059	2.08908	2.72409	6.25706
MCWNT 16	2.49393	3.00657	3.64035	8.02595	2.41209	2.44505	3.92132	9.42588
MCWNT 18	2.60067	3.25619	3.80761	8.97479	2.46953	2.80089	3.61020	8.9986

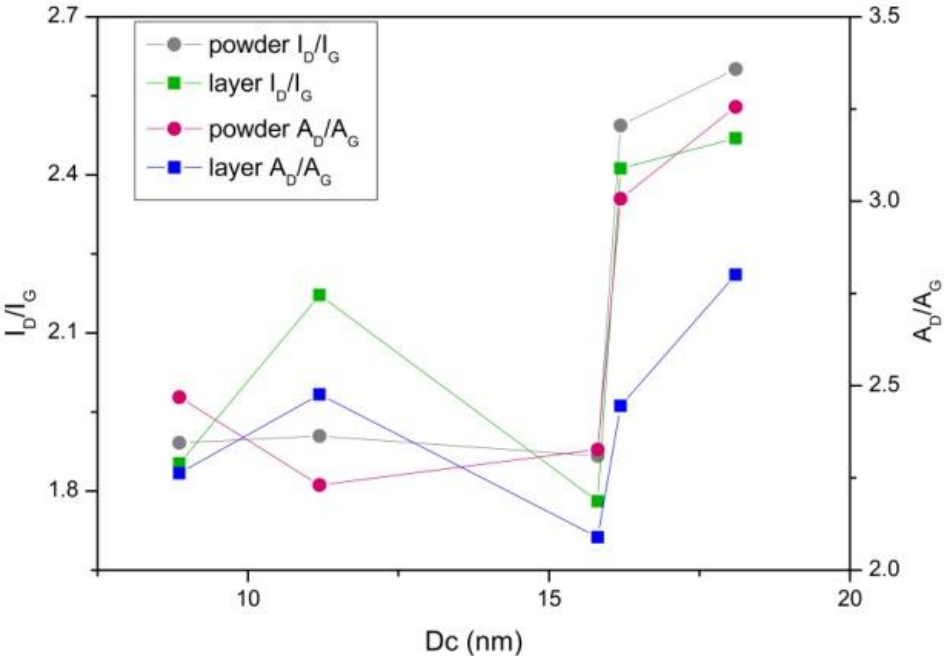

Fig. S5 Intensities (I_D/I_G) and integral intensities (A_D/A_G) ratio of band D and G measured from the powder (circle) and film (square)

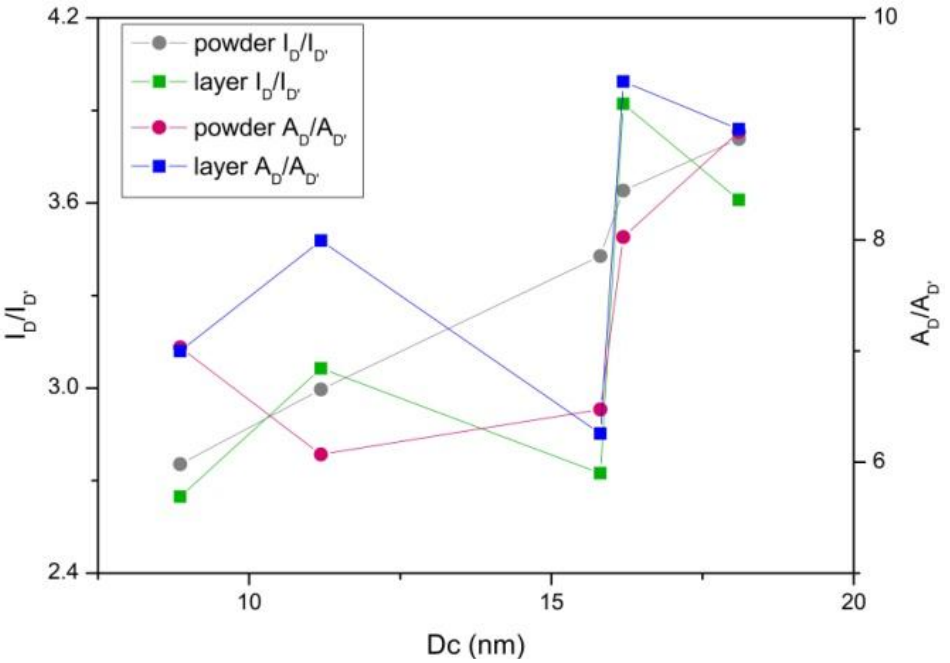

Fig. S6 Intensities ($I_D/I_{D'}$) and integral intensities ($A_D/A_{D'}$) ratio of band D and D' measured from the powder (circle) and film (square)

Surface resistivity anisotropy

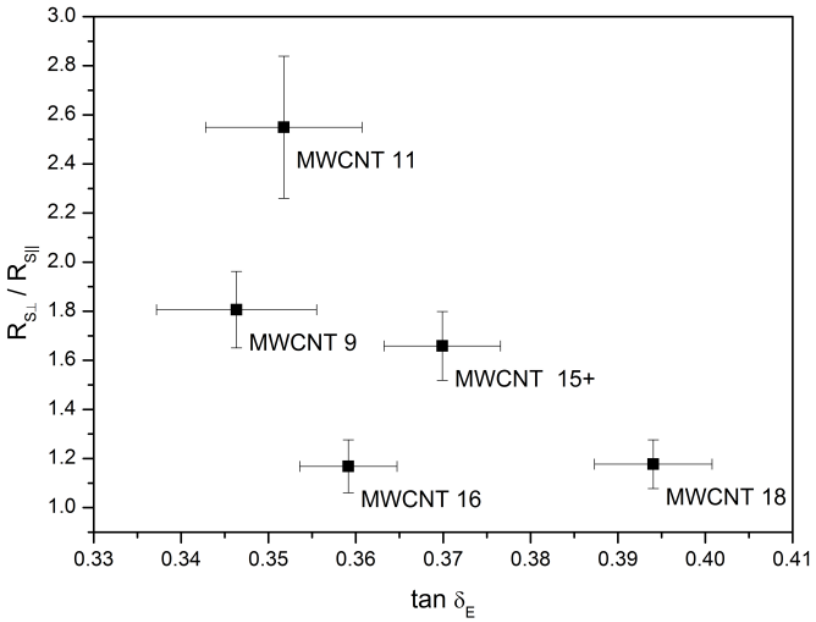

Fig. S7 Dependence of the anisotropy parameter ($\mathbf{R_{S\perp}/\ R_{S\parallel}}$) in the compression loss tangent ($\mathbf{tan\delta_E}$,)